**FIGURE 17.18**

The three atomic bombs of World War II. (a) The “gadget,” an implosion-type plutonium bomb tested in the New Mexico desert on July 16, 1945. (b) The gun-type, called “Little Boy,” dropped on Hiroshima on August 6. (c) The implosion type, called “Fat Man,” dropped on Nagasaki on August 9. The names Little Boy and Fat Man reflect their shapes, which in turn reflect their different functioning as indicated in Fig. 17.17. The Little Boy was 10 feet long and the Fat Man 5 feet in diameter. Both bombs weighed about 5 tons.

Fusion Weapons

Fusion bombs (also called hydrogen, or thermonuclear, bombs) get their enormous destructive power from the fusion of light nuclei. Their principal fuels are the two hydrogen isotopes, deuterium (D) and tritium (T). These isotopes combine in the DD reaction (17.59) and the DT reaction (17.60). As we saw in Section 17.8, the colliding nuclei must have enough energy to overcome their mutual Coulomb repulsion before they can fuse. This requires that the fuel be raised to a temperature between 10 and 100 million kelvins, which is accomplished by using a fission bomb as a “trigger.”

A large explosion also requires that the density of the fuel be higher than is possible with hydrogen gas. The first successful explosion involved building a huge refrigerator plant to liquify the fuel. While the resulting explosion yielded more than 10 megatons, it did not lead to a deliverable bomb since no plane could carry around the needed refrigeration. A smaller bomb was eventually made by solidifying the deuterium into lithium-deuteride (the solid formed of ^6Li and deuterium). This had the additional advantage that, when bombarded by the neutrons from the fission trigger, the ^6Li dissociates into tritium and ^4He , thus furnishing tritium as a fuel and saving the trouble of making and storing radioactive tritium.

17.10 The Theory of Alpha Decay*

*This section could be omitted without loss of continuity.

As we saw in Section 17.5, the naturally occurring radioactive series involve combinations of α and β decays. All three series originate in the α decays of their parent nuclei ^{232}Th , ^{235}U , and ^{238}U . These nuclei exist on earth today only because they have half-lives of billions of years, so that appreciable amounts have survived the billions of years since the formation of our solar system. These extremely long half-lives pose a puzzle: How can a process driven by nuclear energies of millions of electron volts take billions of years to occur?

TABLE 17.1

Five alpha-emitting nuclei in order of decreasing half-life. The second column shows the kinetic energy released in the decay, and the third shows the half-life.

Nucleus	$K(\text{MeV})$	$t_{1/2}$
^{232}Th	4.1	14 billion yr
^{226}Ra	4.9	1600 yr
^{240}Cm	6.4	27 days
^{194}Po	7.0	0.7 s
^{216}Ra	9.5	0.18 μs

The long half-lives of ^{232}Th , ^{235}U , and ^{238}U are not the only puzzles posed by α decay. Table 17.1 shows the half-lives of 5 different α -radioactive nuclei. You can see that the half-lives vary over an astonishing range, from billions of years to fractions of a microsecond, while the energies released range only from about 4 to about 9 MeV. As you can also see, the half-lives are correlated with the energy released: the shorter the half-life, the higher the energy released and vice versa.

Given these facts, the questions we must answer are these: How do nuclei emit alpha particles? Given that they *can* emit alpha particles, why do some nuclei wait more than 10 billion years before doing so? And why is the half-life so extraordinarily sensitive to the energy release K , with a factor of 2 difference in K corresponding to nearly 25 orders of magnitude in $t_{1/2}$? The answers to these questions were found in 1928 by the Russian George Gamow and independently by the Americans Condon and Gurney.

The theory of alpha decay starts from the plausible assumption that two of the protons inside a heavy nucleus can occasionally cluster together with two of the neutrons to form an alpha particle. Experiments* show that this is correct: Alpha particles are continually forming and dissolving inside a nucleus. Averaged over time, it is found that there is of order one alpha particle inside any heavy nucleus.

To find how quickly alpha particles escape from the nucleus, we must first estimate how frequently they appear at the nuclear surface. An alpha particle is formed from four nucleons, each with potential energy about -50 MeV and kinetic energy about 25 MeV. Therefore, the alpha particle should have a kinetic energy of roughly 100 MeV, corresponding to a speed $v \sim c/4$. For a nuclear diameter D of about 15 fm, the frequency with which an alpha particle appears at the surface of the nucleus would be roughly

$$f \sim \frac{v}{D} \sim \frac{c/4}{15 \text{ fm}} \sim 5 \times 10^{21} \text{ s}^{-1} \quad (17.65)$$

We see that alpha particles appear at the nuclear surface more than 10^{21} times per second. We would not necessarily expect these particles to escape since the strong nuclear force pulls them back into the nucleus. Nevertheless, the observed fact is that an alpha particle does occasionally escape. Our task is to see how this occurs and to find the probability of its doing so.

Let us denote by P the probability that a single alpha particle striking the nuclear surface will escape. Our ultimate goal is to find the decay constant, γ ,

George Gamow
(1904–1968, Russian-American)



After various postdoctoral positions in Europe, Gamow settled in the United States. In addition to his theory of alpha decay, he worked out many details of stellar evolution, was an early proponent of the “big-bang” origin of the universe, and was the first to guess (correctly) that the genetic code is carried by triplets of nucleotides. Gamow was also the author of many entertaining books on science.

*For example, reactions involving ejection or transfer of alpha particles from nuclei.

of the nuclei
capping, it is t
with the surf

We have alre

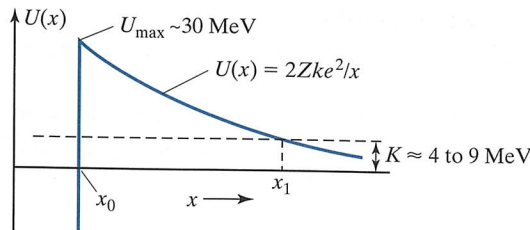
As we l
is given by t
mined by the
potential-enc
sketched in F
fission fragm
cleus, then U
the separatio
the residual i
some x_0 , abo
inates, and th
actly analog
alpha particl
quantum me
and this qua
the barrier ai

To calc
proximate pa
boundary is a
(or, more pre

As can be se
trostatic pote

We kno
moves far aw
9 MeV.* By c
the decay occ
4 and 9 MeV

*We are treati
tion since mc^2
classical energ

**FIGURE 17.19**

The barrier that keeps an alpha particle from escaping promptly from a nucleus. The curve shown is the potential energy $U(x)$ of the alpha particle at a distance x from the center of the offspring nucleus. For $x > x_0$, it is just the Coulomb potential, while for $x < x_0$, it is dominated by the attractive nuclear force and is strongly negative. (The actual curve would be somewhat rounded at x_0 .) The observed kinetic energy when the alpha particle escapes is shown as K .

of the nucleus. Since r is the probability per unit time of an alpha particle escaping, it is the product of f (the frequency with which alpha particles collide with the surface) and P (the probability of escape in any one collision):

$$r = fP \quad (17.66)$$

We have already estimated f in (17.65), and we must now find the probability P .

As we know, the probability of finding a quantum particle in some region is given by the square of its wave function, and the wave function is determined by the Schrödinger equation, whose solution requires knowledge of the potential-energy function. The potential energy of the alpha particle is sketched in Fig. 17.19 and is qualitatively similar to the potential energy of two fission fragments (shown in Fig. 17.14). If the alpha particle is outside the nucleus, then U is just the Coulomb potential energy $U(x) = 2Zke^2/x$, where x is the separation of the alpha from the residual nucleus and Ze is the charge of the residual nucleus. (Remember, the charge of the alpha is $2e$.) For x less than some x_0 , about equal to the nuclear radius R , the attractive nuclear force dominates, and the potential energy drops abruptly. There is therefore a *barrier*, exactly analogous to the fission barrier, and it is this barrier that prevents the alpha particle from escaping instantly. However, as we saw in Section 7.10, quantum mechanics allows a particle to *tunnel* through a barrier of this type, and this **quantum tunneling** is what allows the alpha particle to pass through the barrier and escape.

To calculate the probability of such tunneling, we must establish the approximate parameters of the barrier confining the alpha particle. Its left-hand boundary is at the point shown as x_0 , which is about equal to the nuclear radius (or, more precisely, the sum of the radii of the residual nucleus and the alpha):

$$x_0 \approx 8 \text{ fm}$$

As can be seen in Fig. 17.19, the height U_{\max} of the barrier is simply the electrostatic potential energy at $x = x_0$:

$$U_{\max} = 2Z \frac{ke^2}{x_0} \sim 2 \times 90 \times \frac{1.44 \text{ MeV} \cdot \text{fm}}{8 \text{ fm}} \approx 30 \text{ MeV}$$

We know that when the alpha particle emerges from the nucleus and moves far away, it has kinetic energy and hence total energy between 4 and 9 MeV.* By conservation of energy, this must be the same as its energy before the decay occurred. Therefore, its energy inside the nucleus was also between 4 and 9 MeV (as shown by the dashed horizontal line in Fig. 17.19). This is far

*We are treating the process nonrelativistically, as is certainly an excellent approximation since $mc^2 \approx 4000 \text{ MeV}$ for an alpha particle. Thus “total energy” here means the classical energy, $E = K + U$, and if $U = 0$, then $E = K$.

below the top of the barrier ($U_{\max} \approx 30 \text{ MeV}$) — which confirms that if the alpha were a classical particle inside the nucleus, it would be permanently trapped by the barrier.

Another important parameter shown in Fig. 17.19 is the distance x_1 . This is the separation at which an alpha particle coming *inward* with initial kinetic energy K would be stopped by the barrier. The value of x_1 is determined by the condition

$$2Z \frac{ke^2}{x_1} = K$$

or

$$x_1 = 2Z \frac{ke^2}{K} \approx 2 \times 90 \times \frac{1.44 \text{ MeV} \cdot \text{fm}}{4 \text{ to } 9 \text{ MeV}} \approx 30 \text{ to } 65 \text{ fm}$$

The interval from x_0 to x_1 is the classically forbidden region. Its length, $L = x_1 - x_0$, is the thickness of the barrier through which the alpha particle must tunnel. By nuclear standards, L is rather long and varies appreciably (from roughly 20 to 55 fm as K ranges from 9 down to 4 MeV). We will see that these are the main reasons why the escape probability P is so low and why it varies so much with the energy of the emerging alpha particle.

Barrier Penetration

In Section 7.10 we saw that a quantum particle can pass through a potential-energy barrier that would completely block a classical particle. For a simple rectangular barrier, as shown in Fig. 17.20, we found the probability that a particle which strikes the rectangular barrier of Fig. 17.20 with energy $E < U_0$ will tunnel through and emerge on the outside is

$$P \approx e^{-2\alpha L} \quad (17.67)$$

where

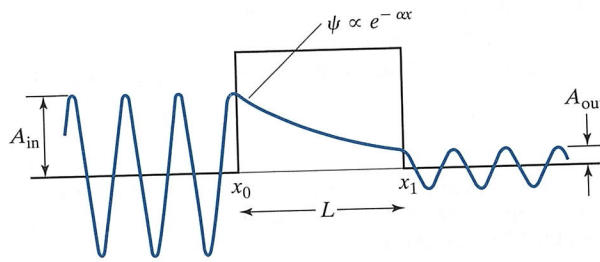
$$\alpha = \sqrt{\frac{2m(U_0 - E)}{\hbar^2}} \quad (17.68)$$

and m is the mass of the particle concerned.

The escape probability (17.67) depends on two variables: α , as given by (17.68), and L , the barrier thickness. If the barrier is high and wide (as is the case in alpha decay), both α and L are large and the escape probability is very small. (Remember that if x is large, e^{-x} is extremely small; for example, if $x = 10$, then $e^{-x} = 0.00005$.) Furthermore, if α is large, $P = e^{-2\alpha L}$ is very

FIGURE 17.20

Wave function for a barrier of finite length. Inside the well ($x < x_0$), $\psi(x)$ is sinusoidal, with amplitude A_{in} ; inside the barrier, it decreases exponentially; then for $x > x_1$, it is sinusoidal again, with amplitude A_{out} .



sensitive to the barrier thickness L . This is the main reason that the observed half-lives vary over such an enormous range.

Equation (17.67) gives the escape probability for any particle confined by a rectangular barrier. Our interest is in an alpha particle confined by the nonrectangular barrier of Fig. 17.19. To find the corresponding escape probability, we can approximate the actual barrier by a succession of n rectangular barriers as in Fig. 17.21. The total escape probability is the product of the n individual probabilities

$$\begin{aligned} P &= P_1 P_2 \cdots P_n \\ &= e^{-2\alpha_1 \Delta x_1} e^{-2\alpha_2 \Delta x_2} \cdots e^{-2\alpha_n \Delta x_n} = \exp\left(-2 \sum \alpha_i \Delta x_i\right) \quad (17.69) \end{aligned}$$

where each α_i is given by (17.68) with the appropriate barrier height U_i . In the limit that all $\Delta x_i \rightarrow 0$, the sum in (17.69) becomes an integral, and we obtain the desired probability,

$$P = \exp\left[-2 \int_{x_0}^{x_1} \alpha(x) dx\right] \quad (17.70)$$

where $\alpha(x)$ is found from (17.68),

$$\alpha(x) = \sqrt{\frac{2m[U(x) - K]}{\hbar^2}} \quad (17.71)$$

by replacing U_0 with $U(x)$ and noting that E is just K , the kinetic energy when the alpha particle is far away from the nucleus and U is zero.

For the case of alpha decay, we know that $U(x) = 2Zke^2/x$, and the integral in (17.70) can be evaluated (Problem 17.60) to give

$$P = \exp\left[-\frac{2\pi ke^2\sqrt{2m}}{\hbar} ZK^{-1/2} + \frac{8\sqrt{mke^2}}{\hbar} (ZR)^{1/2}\right] \quad (17.72)$$

where Z and R denote the charge and radius of the residual nucleus. It is convenient to rewrite this result as

$$P = \exp[-aZK^{-1/2} + b(ZR)^{1/2}] \quad (17.73)$$

where the two constants a and b are easily evaluated (Problem 17.58) to give

$$a = \frac{2\pi ke^2\sqrt{2m}}{\hbar} = 3.97 \text{ (MeV)}^{1/2} \quad (17.74)$$

and

$$b = \frac{8\sqrt{mke^2}}{\hbar} = 2.98 \text{ (fm)}^{-1/2} \quad (17.75)$$

If we substitute the typical values $Z = 90$, $K = 6 \text{ MeV}$, and $R = 8 \text{ fm}$ into (17.73), we find that

$$P \approx \exp(-146 + 80) \approx 2 \times 10^{-29}$$

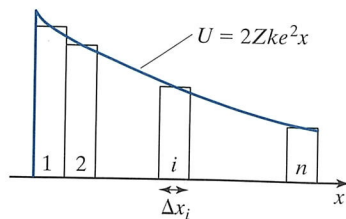


FIGURE 17.21

The actual curved barrier can be approximated as n rectangular barriers, each with thickness Δx_i .

As anticipated, the probability P that an alpha particle striking the surface of a nucleus will escape is extremely small.

Half-Lives

Since experimental data are generally given in terms of half-lives, let us assemble our results to give an expression for the half-life of an alpha-emitting nucleus. The half-life is $(\ln 2)/r$ and the decay constant r is $r = fP$, where f is the frequency with which alpha particles strike the nuclear surface. Therefore,

$$t_{1/2} = \frac{\ln 2}{r} = \frac{0.693}{fP}$$

Since P is given by (17.73) as an exponential, it is convenient to take natural logarithms to give

$$\ln t_{1/2} = -\ln P + \ln \frac{0.693}{f}$$

or, from (17.73),

$$\ln t_{1/2} = aZK^{-1/2} - b(ZR)^{1/2} + c \quad (17.76)$$

In this formula, Z and R are the charge and radius of the residual nucleus. The constants a and b are given by (17.74) and (17.75). The constant c is $\ln(0.693/f)$, where f was estimated as roughly $5 \times 10^{21} \text{ s}^{-1}$ [see (17.65)]; therefore,

$$c = \ln \frac{0.693}{f} \approx -50 \quad (17.77)$$

The simplest way to test our theory is to consider a set of alpha-emitting nuclei that all have the same value of Z . For example, we could consider the isotopes ^{192}Po , ^{194}Po , ^{196}Po , ^{208}Po , ^{210}Po , ^{212}Po , ^{214}Po , ^{216}Po of polonium, all of which decay exclusively by alpha emission.* Since these nuclei all have the same value of Z and very nearly the same radius R , the second term in (17.76) is approximately constant, and (17.76) reduces to

$$\ln t_{1/2} = aZK^{-1/2} + \text{constant} \quad (17.78)$$

That is, our theory of alpha decay predicts that a plot of $\ln t_{1/2}$ against $K^{-1/2}$ for a set of isotopes should be a straight line. The remarkable success of this prediction can be seen in Fig. 17.22, which shows the data for the eight isotopes of polonium mentioned above. The line shown is the least-squares fit to the data. Its slope is 328, in good agreement with the value predicted by (17.78):

$$\text{slope} = aZ = 3.97 \times 82 = 326$$

*We must exclude any isotope with other decay modes in addition to alpha emission, since these reduce $t_{1/2}$. We have also excluded isotopes with A odd since these all have nonzero angular momentum, which (it turns out) complicates the analysis and alters $t_{1/2}$ appreciably.

The line's in
while our pr

(if we take
value, this a
and experim
“constant” c

If we v
ferent elem
vary. Howev
for all resid
important e
Small differ
hence enor
this term is
noted at the

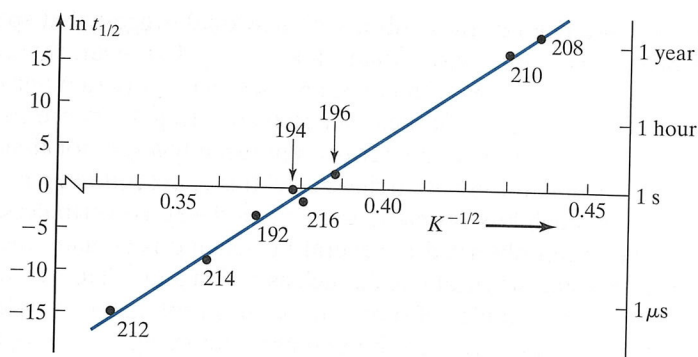
Spontane

We have al
particular, f
occurring i
which incid
pass immed
even withou
when the fi

The p
ry of barrie
angular, th

where

Comparing
we see tha

**FIGURE 17.22**

Plot of $\ln t_{1/2}$ against $K^{-1/2}$ for eight alpha-emitting isotopes of polonium. (Half-lives, $t_{1/2}$, in seconds and energy release, K , in MeV.) The number beside each point is the mass number A of the isotope. The line is the least-squares fit to the data, and the axis on the right shows $t_{1/2}$ itself.

The line's intercept with the vertical axis (not shown in the picture) is at -125 , while our predicted value from (17.78) is

$$\text{"constant"} = -b(ZR)^{1/2} + c \approx -120 \quad (17.79)$$

(if we take $R \approx 7$ fm). Given the rough approximations that went into this value, this agreement is entirely satisfactory. The agreement between theory and experiment is even better if we allow for the small variations of R in the "constant" of (17.79).

If we wish to use the result (17.76) to compute half-lives of various different elements, we must recognize that the three variables K , Z , and R can all vary. However, neither Z nor R varies very much. (For example, $81 \leq Z \leq 90$ for all residual nuclei in the natural radioactive series.) Thus, the single most important effect is still the energy dependence of the term $aZK^{-1/2}$ in $\ln t_{1/2}$. Small differences in K correspond to appreciable differences in this term and hence enormous differences in $t_{1/2}$. In particular, as K ranges from 4 to 9 MeV, this term is the main reason that $t_{1/2}$ drops by some 24 orders of magnitude, as noted at the beginning of this section.

Spontaneous Fission

We have already noted the similarity of alpha decay and nuclear fission. In particular, for both processes, there is a barrier that prevents the decay from occurring instantaneously. In Section 17.7 we discussed *induced fission*, in which incident neutrons produce a nucleus with sufficient excitation energy to pass immediately over the top of the fission barrier. It should now be clear that even without any excitation energy, nuclei should undergo **spontaneous fission** when the fission fragments tunnel through the fission barrier.

The probability of spontaneous fission can be calculated using the theory of barrier penetration. If we suppose, for simplicity, that the barriers are rectangular, the escape probability is given by (17.67) as

$$P \approx e^{-2\alpha L} \quad (17.80)$$

where

$$\alpha = \sqrt{\frac{2m(U_0 - E)}{\hbar^2}} \quad (17.81)$$

Comparing the fission barrier of Fig. 17.14 and the alpha barrier of Fig. 17.19, we see that the fission barrier is somewhat lower ($U_0 - E$ is less) and shorter

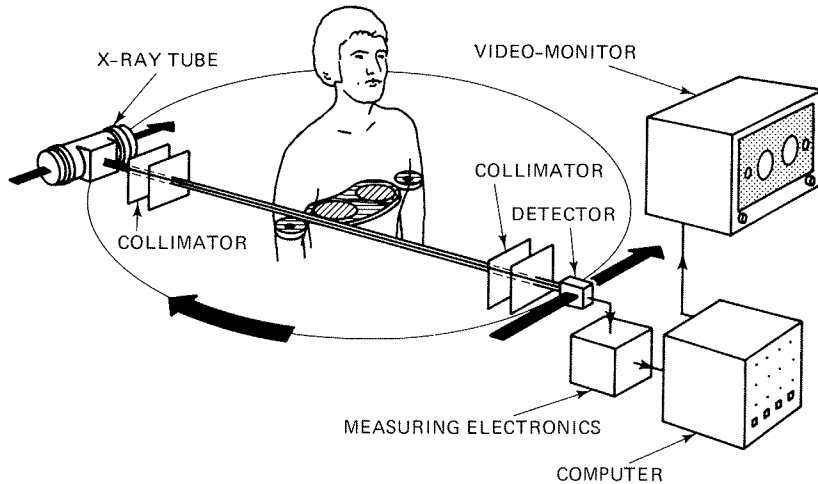


FIG. 7.4 Basic scanning system for computerized tomography. (Courtesy of the Siemens AG-Bereich Medizinische Technik.)

photons are detected by a scanning detector at each position of the scan. This same procedure is repeated at approximately 1° intervals for 180° so that a set of projections are obtained at approximately all angles. The resultant projection data are applied to a digital computer where an accurate two-dimensional image is reconstructed, representing the linear attenuation coefficient in the section of interest. The mathematics involved in the image reconstruction from projection data will be described.

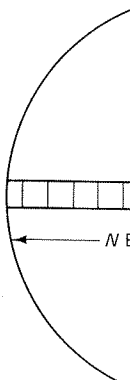
This approach overcomes essentially all of the shortcomings of motion tomography. Only the section of interest is irradiated. Using carefully calibrated detectors, and limited only by the Poisson statistics of the number of counts per measurement, this technique has provided almost uncanny visualization of structures that were previously invisible. Radiologists have been able to perceive lesions whose attenuation coefficient differed by less than 0.5% from the surrounding tissue. Thus, in a noninvasive fashion, an accurate diagnosis is obtained.

RECONSTRUCTION MATHEMATICS— ITERATIVE APPROACHES

The mathematics involved is a relatively old, but seldom used, field of study involving the reconstruction of a two-dimensional distribution from its projections. The most straightforward, although computationally inefficient solution involves linear algebra. The two-dimensional image is reconstructed using a

matrix inversion of the system of equations. This is quite a formidable procedure. This is an iterative process that matches all of the projected data to the measured data. Compared with the more sophisticated algorithms, the initial iteration is slow. It is known as the *Algebraic Reconstruction Technique*, or ART, developed by Brooks and DiChiro, 1

The ART system makes the premise that the results are good enough after a few iterations. The iterative process continues until a constant such as the



the measured data for a given angle θ_j along that ray $\sum_{i=1}^N f_{ij}$ is equal to the j th line forming the projection matrix A among the N reconstructed images.

where the superscript q denotes the values of the elements in the q th row.

As an illustration, consider the values and the associated

matrix inversion of the projection data. For images of reasonable complexity, this is quite formidable. One general class of solutions involves an iterative procedure. This is an attempt to find a two-dimensional distribution that matches all of the projections. An initial distribution is assumed and it is compared with the measured projections. Using one of a variety of iterative algorithms, the initial distribution is successively modified. This method is known as the *Algebraic Reconstruction Technique*, or ART [Herman, 1980; Brooks and DiChiro, 1976a].

The ART system, illustrated in Fig. 7.5, is based on the very general premise that the resultant reconstruction should match the measured projections. The iterative process is started with all reconstruction elements f_i set to a constant such as the mean \bar{f} or zero. In each iteration the difference between

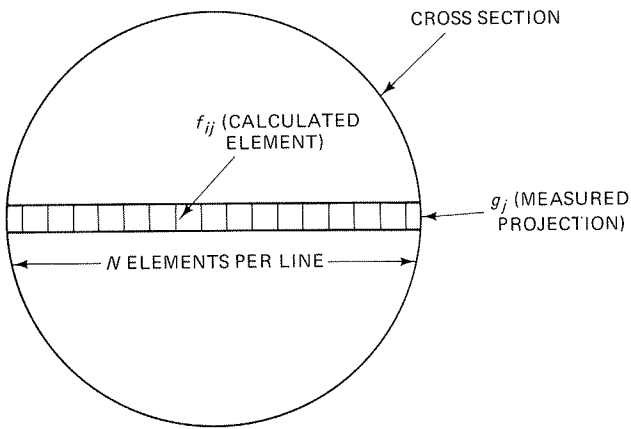


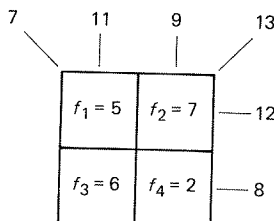
FIG. 7.5 ART system.

the measured data for a projection g_j and the sum of the reconstructed elements along that ray $\sum_{i=1}^N f_{ij}$ is calculated. Here f_{ij} represents an element along the j th line forming the projection ray g_j . This difference is then evenly divided among the N reconstruction elements. The iterative algorithm is defined as

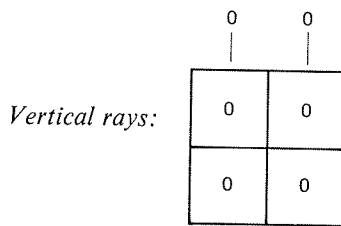
$$f_{ij}^{q+1} = f_{ij}^q + \frac{g_j - \sum_{i=1}^N f_{ij}^q}{N} \quad (7.22)$$

where the superscript q indicates the iteration. The algorithm recursively relates the values of the elements to those of the previous iteration.

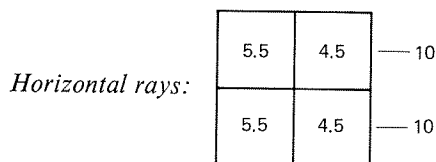
As an illustration of the ART process we use a simple 2×2 matrix of values and the associated measured projections.



All six projection measurements, including the two verticals, two horizontals, and two diagonals, have been made. Presumably, these projection measurements are all that is available and, from these, the matrix of elements shown must be reconstructed. We begin the process arbitrarily by setting all values to zero, calculating the resultant projections, and comparing them to the measured projections. The differences are calculated, divided by the two elements per line, and added to each element.

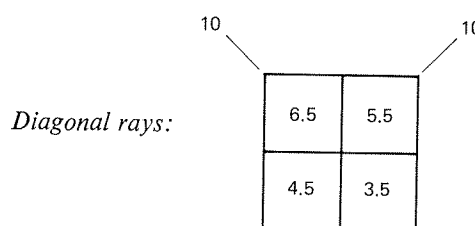


$$f_1^1 = f_3^1 = 0 + \frac{11 - 0}{2} = 5.5; \quad f_2^1 = f_4^1 = 0 + \frac{9 - 0}{2} = 4.5$$



$$f_1^2 = 5.5 + \frac{12 - 10}{2} = 6.5; \quad f_2^2 = 4.5 + \frac{12 - 10}{2} = 5.5$$

$$f_3^2 = 5.5 + \frac{8 - 10}{2} = 4.5; \quad f_4^2 = 4.5 + \frac{8 - 10}{2} = 3.5$$



Thus the original elements are modified after many iterations, using a nonlinear formulation for adequate convergence between the measured and reconstructed values.

A number of variations of the nonlinear formulation are known as *multiplicative ART*, which is *additive ART*. The differences are multiplied by the sum of the reconstructed values.

In multiplicative ART, the magnitude of the difference in the ray is changed at each iteration.

Although the iterative process of computerized tomography by direct methods due to the accuracy in the present reconstruction formulation is slow, it is still useful.

DIRECT RECONSTRUCTION BY FOURIER TRANSFORM

Direct reconstruction methods are illustrated with the aid of the *x* direction, for convenience.

This projection representation is demonstrating the central slice theorem.

$$f_1^3 = 6.5 + \frac{7 - 10}{2} = 5; \quad f_2^3 = 5.5 + \frac{13 - 10}{2} = 7$$

$$f_3^3 = 4.5 + \frac{13 - 10}{2} = 6; \quad f_4^3 = 3.5 + \frac{7 - 10}{2} = 2$$

Thus the original elements are reconstructed. In general, for larger formats, many iterations, using the same measurement data over and over, are required for adequate convergence. The process is usually halted when the difference between the measured and calculated projections is adequately small.

A number of variations on this general theme have been proposed. One nonlinear formulation makes use of the known nonnegativity of the density values f_{ij} . Thus where $f_{ij} < 0$, it is set equal to zero. Another variation is known as *multiplicative ART*, as compared to the previous original algorithm, which is *additive ART*. In the multiplicative version the original density values are multiplied by the ratio of the measured line integral g_j to the calculated sum of the reconstructed elements. This is given by

$$f_{ij}^{q+1} = \frac{g_j}{\sum_{i=1}^N f_{ij}^q} f_{ij}^q. \quad (7.23)$$

In multiplicative ART, each reconstructed element is changed in proportion to its magnitude. This is in sharp contrast to additive ART, where each element in the ray is changed a fixed amount, independent of its magnitude.

Although the iterative methods were the most popular in the earlier days of computerized tomography, they have become almost completely supplanted by direct methods due to problems such as computation time and convergence accuracy in the presence of noise. The direct methods provide a linear reconstruction formulation between a two-dimensional distribution and its projections.

DIRECT RECONSTRUCTION METHODS—FOURIER TRANSFORM APPROACH

Direct reconstruction methods are based on the central section theorem, which is illustrated with the aid of Fig. 7.6. As shown, a single projection is taken in the x direction, for convenience, forming a projection $g(y)$ given by

$$g(y) = \int f(x, y) dx. \quad (7.24)$$

This projection represents an array of line integrals in the x direction. For demonstrating the central section theorem we use the two-dimensional Fourier